Dynamic Surface Control with a Nonlinear Disturbance Observer for Multi-Degree of Freedom Underactuated Mechanical Systems†

Feng Ding[1], Jian Huang*[2], WenXia Xu[3], Chenguang Yang[4], Chong Sun[1], Yong Ai[1]

Abstract: Underactuated systems are extensively utilized in practice while attracting a huge deal of attention in theoretical studies. There are few robust control strategies for general underactuated systems because of the variety of their dynamic models. A dynamic surface control strategy with a nonlinear disturbance observer is proposed in this study, to stabilize multi-degree of freedom underactuated systems. In such systems the number of underactuated degrees of freedom is not higher compared to the actuated ones. A disturbance observer is utilized to dispose of the uncertain disturbance and cross terms in dynamic model which may cause failure to the controller. Then, a dynamic surface control strategy is presented which is not sensitive to the diversity of dynamic models. The stability of whole system is proven by Lyapunov-based method. The control law is successfully applied to nonlinear underactuated systems in benchmark cascade form such as two-Translational Oscillator with Rotational Actuator, Crane, Wheeled Inverted Pendulum. The effectiveness of proposed controllers are illustrated by MATLAB simulation results. Finally, comparative studies are presented to verify the superiority of the proposed method.

Keywords: Dynamic Surface Control, Underactuated Systems, Uniformly Ultimately Bounded, Nonlinear Disturbance Observer

1 Introduction

Stabilizing and tracking control of nonlinear underactuated systems have obtained significant applications in robotic systems. Systems such as acrobot[1, 2], quadrotor[3, 4], cart-pendulum[5], translational oscillator with rotational actuator (TORA)[6, 7], manipulators with structural flexibility [8], wheeled inverted pendulum (MIP)[9, 10], and underactuated surface vessel[11, 12], are modeled as nonlinear underactuated structures. However, it is more complex to design controllers for underactuated systems compared to the full actuated ones. In recent decades, much work has been done on the control of underactuated systems. Various control strategies such as dynamic surface control (DSC)[13, 14, 15, 16], sliding mode control (SMC)[17, 18, 19, 20] , fuzzy control[21, 22], backstepping[23, 24], and adaptive control [25, 26, 27] are proposed for one or a class of underactuated systems.

Among those control strategies, robust control methods such as DSC, SMC are extensively applied to improve the performance and robustness of the underactuated systems because of their less sensitivity to the external disturbance and model uncertainties. However, the robustness of the SMC is obtained by increasing the gain in discontinuous term. Consequently, the chattering problem caused by the discontinuous characteristics of SMC becomes an important factor that make it unable to be applied in the actual systems. A systematic and recursive methodology called DSC proposed by Swaroop [28] overcomes the disadvantage of SMC by introducing a virtual control law. The DSC is initially applied to full actuated nonlinear systems[29, 30, 31, 32]. Recently, the DSC technique are used by some researchers to control the underactuated systems, including the inverted pendulum[13, 33], and the autonomous surface vehicles[14]. A T-S fuzzy adaptive DSC is utilized to meet the objective of ball positioning subjected to parameter uncertainties for a ball and beam system [15] . Based on the linear model of a class of two-degree of freedom (two-DOF) underactuated systems, a gain scheduled DSC (GSDSC) was developed by introducing a neural network disturbance observer with adaptive law to estimate uncertainties[16]. However, when the initial states are far away from the equilibrium, it may be failed or sensitive to the parameters.

There are some studies on a specific underactuated system [13, 14, 15, 33] or a certain class of underactuated systems[34, 35]. However, little work is performed on general underactuated systems, especially general multi-DOF underactuated systems. The main difficulty is that underactuated systems can not be described by standard models satisfying the special requirements in the controller design. The general cascade form of underactuated systems may contain nonlinear functions or cross items causing computing feasibility problem in the process of controller derivation. On the other hand, algorithms for two-DOF underactuated systems may not be available for multi-DOF underactuated systems if computing problems are occurred such as the inverse of non-square matrix, multiplication of matrices with different dimensions [7, 16].

†This work was supported by the National Natural Science Foundation of China under Grants 61803286 and U1913207; the Natural Science Foundation of Hubei Province of China under Grant 2021CFB258; the Technology Innovation Project of Hubei Province of China under Grant 2019AEA171; and the Fundamental Research Funds for the Central Universities (South-Central Minzu University, Grant No. CZY19015). This work was also supported in part by the Joint fund of Science and Technology Department of Liaoning Province and State Key Laboratory of Robotics, China (Grant No. 2020-KF-22-01)

[1] School of Computer Science, South-Central Minzu University,Hubei,China

[2]Key Laboratory of Image Processing and Intelligent Control, School of Artificial Intelligence and Automation, Huazhong University of Science and Technology,Hubei,China

[3]School of Computer Science and Engineering, Wuhan Institute of Technology,Hubei,China

[4]Bristol Robotics Laboratory, University of the West of England,Bristol,U.K.

* Corresponding author: Jian Huang Email:huang_jan@mail.hust.edu.cn

In this paper, to reduce the effects of the diversity of models, we propose a nonlinear disturbance observer (NDO) based control strategy. Besides external disturbance, the cross items which can not meet the controller design requirements are considered as disturbance and estimated by the NDO to avoid the computing feasibility problem. The disturbance observer was originally proposed by Chen[36] and rapidly developed in recent years. NDO[2], fuzzy logic observer[37, 38], sliding mode disturbance observer[39], radial basis function neural network observer[16] have already been applied in underactuated systems. It was proven that an NDO can estimate a continuous disturbance which is considered to be a part of system in the controller design[2].

A dynamic surface controller with a nonlinear disturbance observer (DSCNDO) is proposed for the general underactuated systems where the number of underactuated DOFs is no more than that of actuators. The main contributions of our work include: 1) An NDO-based strategy is proposed to reduce the effects of model diversities of underactuated system and to estimate the external disturbance. 2) A novel DSCNDO with simpler deriving process and less parameters ensure states uniformly ultimately bounded. 3) The proposed strategy is applied to nonlinear underactuated systems in benchmark cascade form such as two-TORA, Crane and WIP successfully.

The main structure of this paper is as follows. The control problem of a general underactuated system modeled by Lagrange method is presented in Section 2. In Section 3, A DSCNDO is derived based on the cascade form of dynamic model with external disturbance. Then, the convergence of the entire system is proven by Lyapunov-based analysis. To demonstrate the theoretical analysis, application examples and simulation results with comparison studies are presented in Section 4. Ultimately, the brief concluding remarks are provided in Section 5.

2 Underactuated Systems Description

2.1 Problem Statement

In this paper, we take into account the mechanical systems with n-DOF. The dynamics is derived by Lagrangian equations

$$\frac{d}{dt}(\frac{\partial K}{\partial \dot{q}_i}) - \frac{\partial K}{\partial q_i} + \frac{\partial P}{\partial q_i} + \frac{\partial \Psi}{\partial \dot{q}_i} = \tau_i + d_i$$

where K, P, Ψ are kinetic energy, potential energy, dissipative energy respectively; q_i is the generalized coordinate; τ_i is the generalized force; d_i includes model uncertainties and external disturbance.

The dynamics of underactuated systems derived by Lagrange-based method can be detailed as follows:

$$\begin{array}{l} m_{11}(q)\ddot{q}_1 + m_{12}(q)\ddot{q}_2 + m_{13}(q)\ddot{q}_3 + h_1(q,\dot{q}) = \tau_1 + d_1 \\ m_{21}(q)\ddot{q}_1 + m_{22}(q)\ddot{q}_2 + m_{23}(q)\ddot{q}_3 + h_2(q,\dot{q}) = \tau_2 + d_2 \\ m_{31}(q)\ddot{q}_1 + m_{32}(q)\ddot{q}_2 + m_{33}(q)\ddot{q}_3 + h_3(q,\dot{q}) = \tau_3 + d_3 \end{array} \tag{1}$$

where $q = [q_1, q_2, q_3]^T$, $q_1 \in R^m, q_2 \in R^m, q_3 \in R^{(n-2m)}$, $(n - 2m \geq 0)$. h_1, h_2 contain Coriolis, centrifugal and gravity terms. τ_1 and τ_2 are the control inputs meeting either of the following conditions[40].

$C1)$ $\tau_1 = 0$ & $\tau_2 = \tau$, q_1 is underactuated. τ, τ_3 are the inputs.

$C2)$ $\tau_2 = 0$ & $\tau_1 = \tau$, q_2 is underactuated. τ, τ_3 are the inputs.

Remark 1 Some mechanics, such as quadrotor-slung payload system , wheeled inverted pendulum, and autonomous underwater vehicles, satisfy $n - 2m > 0$. Some systems such as, acrobot, crane and TORA, satisfy $n - 2m = 0$. In this case, the third equation in (1) and the following deduction related to q_3 can be ignored.

2.2 Cascade Normal Form

The dynamics of underactuated system obtained from the Lagrangian equation can be transformed into cascade system with structural features.

Global change of coordinates are chosen as:

$$\begin{array}{ll} x_1 = q_1 + \beta & \\ x_2 = m_{11}\dot{q}_1 + m_{12}\dot{q}_2 + m_{13}\dot{q}_3 & (for\ C1) \\ (x_2 = m_{21}\dot{q}_1 + m_{22}\dot{q}_2 + m_{23}\dot{q}_3 & (for\ C2)) \\ x_3 = q_2 & \\ x_4 = \dot{q}_2 & \\ x_5 = q_3 & \\ x_6 = \dot{q}_3 & \end{array} \tag{2}$$

where $\beta = \int m_{11}^{-1}(m_{12}\dot{q}_2 + m_{13}\dot{q}_3)dt$ for case $C1$, $\beta = \int m_{21}^{-1}(m_{22}\dot{q}_2 + m_{23}\dot{q}_3)dt$ for case $C2$.

Then, convert the dynamics of (1) into a cascade form.

$$
\begin{aligned}
&\dot{x}_1 = \dot{q}_1 + m_{11}^{-1}(m_{12}\dot{q}_2 + m_{13}\dot{q}_3) = m_{11}^{-1}x_2 \ (for \ \ C1) \\
&(\dot{x}_1 = \dot{q}_1 + m_{21}^{-1}(m_{22}\dot{q}_2 + m_{23}\dot{q}_3) = m_{21}^{-1}x_2 \ (for \ \ C2)) \\
&\dot{x}_2 = \frac{d}{dt}(m_{11}\dot{q}_1 + m_{12}\dot{q}_2 + m_{13}\dot{q}_3) = f_1 + D_1 \ (for \ \ C1) \\
&(\dot{x}_2 = \frac{d}{dt}(m_{21}\dot{q}_1 + m_{22}\dot{q}_2 + m_{23}\dot{q}_3) = f_1 + D_1 \ (for \ \ C2)) \\
&\dot{x}_3 = x_4 \\
&\dot{x}_4 = f_2 + b_1 u + D_2 \\
&\dot{x}_5 = x_6 \\
&\dot{x}_6 = f_3 + b_2 u + D_3
\end{aligned} \tag{3}
$$

where $u = [\tau, \tau_3]$, $f_2, f_3, b_1, b_2, D_1, D_2, D_3$ can be extracted by the matrix operation in (1).

Without loss of generality, case $C1$ is taken as an example in the following deduction. For simplicity, (3) can be structured as the vector form.

$$
\dot{X} = F_1(X) + G_1(X)u + G_2 d \tag{4}
$$

where $X = [x_1, x_2, x_3, x_4, x_5, x_6]^T, d = [D_1, D_2, D_3]^T$,

$$
F_1 = \begin{bmatrix} m_{11}^{-1}x_2 \\ f_1 \\ x_4 \\ f_2 \\ x_6 \\ f_3 \end{bmatrix}, G_1 = \begin{bmatrix} 0 \\ 0 \\ 0 \\ b_1 \\ 0 \\ b_2 \end{bmatrix}, G_2 = \begin{bmatrix} 0 & 0 & 0 \\ I_1 & 0 & 0 \\ 0 & 0 & 0 \\ 0 & I_1 & 0 \\ 0 & 0 & 0 \\ 0 & 0 & I_2 \end{bmatrix}
$$

$I_1 \in R^{m\times m}, I_2 \in R^{(n-2m)\times(n-2m)}$ are identity matrices.

Remark 2 The dynamic model (1) is obtained through Lagrangian method. f_1 contains gravity items (related to x_3), dissipative terms (related to x_4), even cross items. The condition that $\partial f_1/\partial x_3$ or $\partial f_1/\partial x_4$ is invertible is not necessarily satisfied when the cross item exists. In this case, $\partial f_1/\partial x_3$ and $\partial f_1/\partial x_4$ are irreversible at the original point.

3 Dynamic Surface Control Strategy for Underactuated Systems

In this section, a dynamic surface controller with a disturbance observer is presented for underactuated systems in cascade form.

3.1 Nonlinear Disturbance Observer

It was proven that the disturbance observer can estimate continuous differentiable uncertainties[2]. Considering the underactuated dynamics (4) with continuous disturbance, the rth-order derivative of d satisfying $\|d^{(r)}\| \le \mu$, where $\mu > 0$ is a constant, construct a (r-1)-order nonlinear disturbance observer:

$$
\begin{cases} \hat{d}^{(i-1)} = z_i + p_i(X) \\ \dot{z}_i = L_i(-F_1(X) - G_1(X)u - G_2\hat{d}) + \hat{d}^{(i)} \end{cases}
\begin{cases} \hat{d}^{(r-1)} = z_r + p_r(X) \\ \dot{z}_r = L_r(-F_1(X) - G_1(X)u - G_2\hat{d}) \end{cases} \tag{5}
$$

where $i = 1, 2, \cdots, r-1$.

The gain matrix L_i is determined as $L_i = \partial p_i(X)/\partial X$.

Define the estimation error of ith-order of d as $\tilde{d}^{(i)} = d^{(i)} - \hat{d}^{(i)}$.

The derivative of $\tilde{d}^{(i-1)}$ is:

$$
\begin{aligned}
\dot{\tilde{d}}^{(i-1)} &= d^{(i)} - \dot{\hat{d}}^{(i-1)} \\
&= d^{(i)} - L_i(-F_1(X) - G_1(X)u - G_2\hat{d}) - \hat{d}^{(i)} - L_i\dot{X} \\
&= d^{(i)} - L_i G_2 \tilde{d} - \hat{d}^{(i)} \\
&= \tilde{d}^{(i)} - L_i G_2 \tilde{d}
\end{aligned}
$$

The derivative of $\tilde{d}^{(r-1)}$ is:

$$
\begin{aligned}
\dot{\tilde{d}}^{(r-1)} &= d^{(r)} - \dot{\hat{d}}^{(r-1)} \\
&= d^{(r)} - L_r G_2 \tilde{d}
\end{aligned}
$$

Define an error vector $D = [\tilde{d}, \dot{\tilde{d}}, \cdots, \tilde{d}^{(r-1)}]^T$. We have:

$$\dot{D} = AD + Id^{(r)} \tag{6}$$

where

$$A = \begin{bmatrix} -L_1G_2 & \mathbf{I_n} & \mathbf{0} & \cdots & \mathbf{0} \\ -L_2G_2 & \mathbf{0} & \mathbf{I_n} & \cdots & \mathbf{0} \\ \vdots & \vdots & \vdots & \vdots & \vdots \\ -L_{r-2}G_2 & \mathbf{0} & \mathbf{0} & \cdots & \mathbf{I_n} \\ -L_{r-1}G_2 & \mathbf{0} & \mathbf{0} & \cdots & \mathbf{0} \end{bmatrix}, I = \begin{bmatrix} \mathbf{0} \\ \mathbf{0} \\ \vdots \\ \mathbf{0} \\ \mathbf{I_n} \end{bmatrix}$$

$I_n \in R^{n\times n}$ is an identity matrix.

Choose appropriate L_i to satisfy matrix A negative definite. The (r-1)-order nonlinear disturbance observer (5) ensures the disturbance tracking error uniformly ultimately bounded if $d^{(r)}$ is bounded. The nonlinear disturbance observer (5) ensures the disturbance tracking error asymptotically stable if $d^{(r)} = 0$.

3.2 Dynamic Surface Controller Design based on a Nonlinear Disturbance Observer

The errors are defined as:

$e_{11} = x_1 - x_{1d}$, $e_{12} = x_2 - x_{2d}, e_{13} = \dot{x}_2 - \dot{x}_{2d}, e_{14} = \dot{f}_1 - \dot{f}_{1d}, e_{21} = x_5 - x_{5d}, e_{22} = x_6 - x_{6d}$.

where $x_{1d}, x_{2d}, \dot{x}_{2d}, \dot{f}_{1d}, x_{5d}, x_{6d}$ are the desired value of $x_1, x_2, \dot{x}_2, \dot{f}_1, x_5, x_6$, respectively.

Following the lines of dynamic surface controller design, $\dot{x}_4$ and $\dot{x}_6$ should be included in the second dynamic surface. To meet the requirement, when f_1 related to x_4 satisfies $\partial f_1/\partial x_4 \neq 0$, e_{14} is excluded in the second dynamic surface, otherwise, e_{14} is included.

Near the equilibrium, three cases are discussed, one each for $\partial f_1/\partial x_4 = 0$ & $\partial f_1/\partial x_3 \neq 0$; $\partial f_1/\partial x_4 \neq 0$; $\partial f_1/\partial x_4 = \partial f_1/\partial x_3 = 0$.

Case 1: $\partial f_1/\partial x_4 = 0$, $\partial f_1/\partial x_3$ is invertible.

There are two stages for designing dynamic surface controller.

1) Designing the virtual control law

The first dynamic surface is defined as:

$$\begin{cases} S_{11} = c_{11}e_{11} + c_{12}e_{12} + e_{13} \\ S_{21} = e_{21} \end{cases} \tag{7}$$

where c_{11}, c_{12} are positive constants.

The derivations of S_{11}, S_{21} are stated as:

$$\begin{cases} \dot{S}_{11} = c_{11}m_{11}^{-1}x_2 + c_{12}(f_1 + D_1) + \dot{f}_1 + \dot{D}_1 - X_{1d} \\ \dot{S}_{21} = x_6 - x_{6d} \end{cases} \tag{8}$$

where $X_{1d} = c_{11}m_{11d}^{-1}x_{2d} + c_{12}(f_{1d} + \hat{D}_1) + \dot{f}_{1d} + \hat{\dot{D}}_1$. $\hat{D}_1, \hat{\dot{D}}_1$ are the estimations of D_1 and $\dot{D}_1$, respectively.

The virtual control law is determined as:

$$\begin{cases} \alpha_1 = -k_{11}S_{11} \\ \alpha_2 = -k_{21}S_{21} \end{cases} \tag{9}$$

where k_{11}, k_{21} are constants.

Input α_1, α_2 to first-order filters.

$$\begin{cases} T_1\dot{\alpha}_{f1} + \alpha_{f1} = \alpha_1 \\ T_2\dot{\alpha}_{f2} + \alpha_{f2} = \alpha_2 \end{cases} \tag{10}$$

where T_1, T_2 are the filter time constants.

The filter errors are determined as:

$$\begin{cases} e_1 = \alpha_{f1} - \alpha_1 \\ e_2 = \alpha_{f2} - \alpha_2 \end{cases} \tag{11}$$

Integrating (9) and (11), we have:

$$\begin{cases} e_1 = \alpha_{f1} + k_{11}S_{11} \\ e_2 = \alpha_{f2} + k_{21}S_{21} \end{cases} \tag{12}$$

2) Designing the actual control law

The second dynamic surface is defined as:

$$\begin{cases} S_{12} = c_{11}m_{11}^{-1}e_{12} + c_{12}e_{13} + e_{14} + \hat{\dot{D}}_1 - \alpha_{f1} \\ S_{22} = e_{22} - \alpha_{f2} \end{cases} \tag{13}$$

Then, the derivatives of S_{12}, S_{22} can be stated as:

$\dot{S}_{12} = c_{11}m_{11}^{-1}\dot{x}_2 + c_{11}\frac{dm_{11}^{-1}}{dt}x_2 + c_{12}(\dot{f}_1 + \dot{D}_1) + \ddot{f}_1 + \dot{\hat{D}}_1 - \dot{X}_{1d} - \dot{\alpha}_{f1}$

$= c_{11}m_{11}^{-1}(f_1+D_1)+c_{11}\frac{dm_{11}^{-1}}{dt}x_2+c_{12}(\frac{\partial f_1}{\partial x_1}m_{11}^{-1}x_2+\frac{\partial f_1}{\partial x_3}x_4+\frac{\partial f_1}{\partial x_5}x_6+\dot{D}_1)+\frac{\partial f_1}{\partial x_1}m_{11}^{-1}(f_1+D_1)+\frac{d}{dt}(\frac{\partial f_1}{\partial x_1}m_{11}^{-1})x_2+$
$\frac{d}{dt}\frac{\partial f_1}{\partial x_3}x_4+\frac{d}{dt}\frac{\partial f_1}{\partial x_5}x_6+\frac{\partial f_1}{\partial x_3}(f_2+b_1u+D_2)+\frac{\partial f_1}{\partial x_5}(f_3+b_2u+D_3)+\dot{\hat{D}}_1-\dot{\alpha}_{f1}-c_{11}\frac{dm_{11}^{-1}}{dt}x_{2d} - c_{11}m_{11}^{-1}(f_{1d} + \hat{D}_1) - c_{12}(\dot{f}_{1d} + \dot{\hat{D}}_1) -$

$\dot{S}_{22} = f_3 + b_2u + D_3 - \dot{\alpha}_{f2} - \dot{x}_{6d}$

Select the dynamic surface controller as:

$$u = -B^{-1}\begin{bmatrix} \Upsilon_1 \\ \Upsilon_2 \end{bmatrix} \tag{14}$$

where

$B = \begin{bmatrix} \frac{\partial f_1}{\partial x_3}b_1 + \frac{\partial f_1}{\partial x_5}b_2 \\ b_2 \end{bmatrix}$

$\Upsilon_1 = c_{11}m_{11}^{-1}f_1 + c_{11}\frac{dm_{11}^{-1}}{dt}x_2 + c_{12}(\frac{\partial f_1}{\partial x_1}m_{11}^{-1}x_2 + \frac{\partial f_1}{\partial x_3}x_4 + \frac{\partial f_1}{\partial x_5}x_6) + \frac{\partial f_1}{\partial x_1}m_{11}^{-1}f_1 + \frac{d}{dt}(\frac{\partial f_1}{\partial x_1}m_{11}^{-1})x_2 + \frac{d}{dt}\frac{\partial f_1}{\partial x_3}x_4 +$
$\frac{\partial f_1}{\partial x_3}f_2 + \frac{d}{dt}\frac{\partial f_1}{\partial x_5}x_6 + \frac{\partial f_1}{\partial x_5}f_3 + \delta_1\hat{D}_1 + \delta_2\hat{D}_2 + \delta_3\hat{D}_3 + k_{12}S_{12} - \frac{\alpha_1 - \alpha_{f1}}{T_1} - c_{11}\frac{dm_{11}^{-1}}{dt}x_{2d} - c_{11}m_{11}^{-1}f_{1d} - c_{12}\dot{f}_{1d} - \ddot{f}_{1d}$

$\Upsilon_2 = f_3 + k_{22}S_{22} + \hat{D}_3 - \frac{\alpha_2 - \alpha_{f2}}{T_2} - \dot{x}_{6d}$

k_{12}, k_{22} are positive constants. $\delta_1 = \frac{\partial f_1}{\partial x_1}m_{11}^{-1}, \delta_2 = \frac{\partial f_1}{\partial x_3}, \delta_3 = \frac{\partial f_1}{\partial x_5}$.

Theorem Considering the underactuated system (4), when $\partial f_1/\partial x_4 = 0$ and B is invertible, a set of surface gains k_1, k_2 and the filter time constant vector T satisfying

$$\gamma = min\{\underline{k_1} - \frac{9}{4}, \underline{k_2} - \frac{5}{4}, \frac{1}{\overline{T}} - 2\} > 0 \tag{15}$$

the DSCNDO (14) ensures that the states are uniformly ultimately bounded.
where $\underline{k_1}, \underline{k_2}$ are the minimum elements of k_1 and k_2, respectively. $\overline{T}$ represents the maximum elements of T. $k_1 = diag(k_{11}, k_{21})$, $k_2 = diag(k_{12}, k_{22}), T = diag(T_1, T_2)$.

proof. Choosing Lyapunov candidate:

$$V = V_1 + V_2 \tag{16}$$

where $V_1 = \tilde{D}^T P\tilde{D}$, $\tilde{D}$ is the disturbance tracking error defined as $\tilde{D} = \begin{bmatrix}\tilde{d} & \tilde{\dot{d}}, \cdots, \tilde{d}^{(r-1)}\end{bmatrix}^T$. P represents a positive definite matrix. $V_2 = \frac{1}{2}S_1^TS_1 + \frac{1}{2}S_2^TS_2 + \frac{1}{2}e^Te$. $S_1 = [S_{11} \quad S_{21}]^T, S_2 = [S_{12} \quad S_{22}]^T, e = [e_1 \quad e_2]^T$

Differentiating both sides of V_1 and replacing (5)-(6) into it, we have[2]:

$$\dot{V}_1 = \tilde{D}^T(A^TP + PA^T)\tilde{D}^T + 2\tilde{D}^TPId^{(r)}$$

A defined in (6) is a negative definite matrix satisfying $A^TP + PA^T = -Q$, where Q is a positive defined matrix. We have:

$$\dot{V}_1 \leq \quad -\lambda V_1 + 2\|\tilde{D}\|\|PId^{(r)}\| \tag{17}$$

where λ is the minimum eigenvalue of Q.

The tracking error $\tilde{D}$ exponentially converges to zero if $d^{(r)} = 0$. $\tilde{D}$ is uniformly ultimately bounded if $d^{(r)}$ is bounded.

Differentiating both sides of V_2 and replacing (8)- (14) into it, we have

$$\begin{aligned}
&\dot{V}_2 = S_1^T\dot{S}_1 + S_2^T\dot{S}_2 + e^T\dot{e} \\
&= S_1^T\begin{bmatrix} S_{12} + \tilde{\dot{D}}_1 + e_1 - k_{11}S_{11} \\ S_{22} + e_2 - k_{21}S_{21} \end{bmatrix} + S_2^T\begin{bmatrix} -k_{12}S_{12} + \kappa_1 \\ -k_{22}S_{22} + \kappa_2 \end{bmatrix} + e^T\begin{bmatrix} -T_1^{-1}e_1 + k_{11}\dot{S}_{11} \\ -T_2^{-1}e_2 + k_{21}\dot{S}_{21} \end{bmatrix} \\
&\leq -S_1^Tk_1S_1 - S_2^Tk_2S_2 - e^TT^{-1}e + S_1^Te + S_1^TS_2 + |S_1^T\bar{\eta}| + |S_2^T\bar{\kappa}| + e^Tk_1\dot{S}_1
\end{aligned} \tag{18}$$

where $\eta = [\tilde{\dot{D}}_1, 0]^T$, $\kappa_1 = (\delta_1 + c_{11}m_{11}^{-1})\tilde{D}_1 + \delta_2\tilde{D}_2 + \delta_3\tilde{D}_3 + c_{12}\tilde{\dot{D}}_1, \kappa_2 = \tilde{D}_3$, $\kappa = [\kappa_1, \kappa_2]^T$, $\tilde{\dot{D}} = \dot{D} - \dot{\hat{D}}, \tilde{D}_i = D_i - \hat{D}_i$. $\bar{\eta}$, $\bar{\kappa}$ are the upper bounds of η and κ , respectively.

It should be noted that $k_1\dot{S}_1$ can be dominated by a continuous functions ρ, that is :

$$|k_1\dot{S}_1| = |k_1(S_2 + e - k_1S_1 + \eta)| \leq \rho(e, S_1, S_2, \tilde{\dot{D}}_1)$$

Based on the Young's inequality, we have:

$$\begin{cases} S_1^T e \le e^T e + S_1^T S_1/4 \\ S_1^T S_2 \le S_1^T S_1 + S_2^T S_2/4 \\ |S_1^T \bar{\eta}| \le S_1^T S_1 + \bar{\eta}^T \bar{\eta}/4 \\ |S_2^T \bar{\kappa}| \le S_2^T S_2 + \bar{\kappa}^T \bar{\kappa}/4 \\ |e^T \rho| \le e^T e + \rho^T \rho/4 \end{cases} \tag{19}$$

Since any constant $p > 0$, set $\Pi = \{(e, S_1, S_2, \eta) = e^T e + S_1^T S_1 + S_2^T S_2 + \tilde{\dot{D}}_1^T \tilde{\dot{D}}_1 \le 2p\}$ is compacted in R^4. Thus, the continuous function ρ possesses a maximum ϱ. Thus,

$$\dot{V}_2 \le -(\underline{k_1} - \frac{9}{4})S_1^T S_1 - (\underline{k_2} - \frac{5}{4})S_2^T S_2 - (\frac{1}{\overline{T}} - 2)e^T e + \frac{1}{4}\varrho^T \varrho + \frac{1}{4}\bar{\kappa}^T \bar{\kappa} + \frac{1}{4}\bar{\eta}^T \bar{\eta} \tag{20}$$

By satisfying the inequalities, $\underline{k_1} - \frac{9}{4} > 0, \underline{k_2} - \frac{5}{4} > 0, \frac{1}{\overline{T}} - 2 > 0$, we have:

$$\dot{V}_2 \le -2\gamma V_2 + \Gamma$$

where $\Gamma = \frac{1}{4}\bar{\kappa}^T \bar{\kappa} + \frac{1}{4}\varrho^T \varrho + \frac{1}{4}\bar{\eta}^T \bar{\eta}$

By choosing appropriate parameters k_1, k_2, T to satisfy (15), we can make $\gamma > \Gamma/2p$. If $V_2(0) \le p$, $V_2(t) \le p$. Accordingly, S_1, S_2, e are bounded. So are e_{21}, e_{22}.

Assuming that a constant matrix χ satisfies $S_{11} = \chi$, thus, $e_{13} = -c_{11}e_{11} - c_{12}e_{12} + \chi$, we have:

$$\begin{bmatrix} \dot{e}_{11} \\ \dot{e}_{12} \end{bmatrix} = M \begin{bmatrix} e_{11} \\ e_{12} \end{bmatrix} + \begin{bmatrix} 0 \\ \chi \end{bmatrix} \tag{21}$$

where

$$M = \begin{bmatrix} 0 & m_{11}^{-1} \\ -c_{11} & -c_{12} \end{bmatrix}$$

Choose appropriate c_{11}, c_{12} to satisfy the eigenvalues of M negative. e_{11}, e_{12} are bounded and converge exponentially to the origin adjacent. So are e_{13}, e_{14}

According to the above analysis, the state tracking errors $e_{11}, e_{12}, e_{13}, e_{14}, e_{21}, e_{22}$ and disturbance tracking error $\tilde{D}$ are uniformly ultimately bounded. Hence, the proof is completed.

Case 2: $\partial f_1/\partial x_4$ is invertible.

The first dynamic surface is chosen as:

$$S_{11} = c_{11}e_{11} + e_{12} \tag{22}$$

Following the lines from (8)-(13), the second dynamic surface is defined as:

$$S_{12} = c_{11}m_{11}^{-1}e_{12} + e_{13} - \alpha_{f1} \tag{23}$$

S_{21}, S_{22} are selected as those in the second equation of (7) and (13), respectively.

Then, the derivative of S_{12} can be expressed as

$$\begin{aligned} \dot{S}_{12} &= c_{11}m_{11}^{-1}\dot{x}_2 + c_{11}\frac{dm_{11}^{-1}}{dt}x_2 + \dot{f}_1 + \dot{D}_1 - \dot{\alpha}_{f1} - c_{11}\frac{dm_{11}^{-1}}{dt}x_{2d} - c_{11}m_{11}^{-1}(f_{1d} + \hat{D}_1) - \dot{f}_{1d} - \dot{\hat{D}}_1 \\ &= c_{11}m_{11}^{-1}(f_1 + D_1) + c_{11}\frac{dm_{11}^{-1}}{dt}x_2 + \frac{\partial f_1}{\partial x_1}m_{11}^{-1}x_2 + \frac{\partial f_1}{\partial x_2}(f_1 + D_1) + \frac{\partial f_1}{\partial x_3}x_4 + \frac{\partial f_1}{\partial x_4}(f_2 + b_1u + D_2) + \frac{\partial f_1}{\partial x_5}x_6 \\ &+ \frac{\partial f_1}{\partial x_6}(f_3 + b_2u + D_3) + \dot{D}_1 - \dot{\alpha}_{f1} - c_{11}\frac{dm_{11}^{-1}}{dt}x_{2d} - c_{11}m_{11}^{-1}(f_{1d} + \hat{D}_1) - \dot{f}_{1d} - \dot{\hat{D}}_1 \end{aligned} \tag{24}$$

According to (24) and $\dot{S}_{22}$ in *Case 1*, we have the following control law:

$$u = -B^{-1} \begin{bmatrix} \Upsilon_1 \\ \Upsilon_2 \end{bmatrix} \tag{25}$$

where

$$B = \begin{bmatrix} \frac{\partial f_1}{\partial x_4}b_1 + \frac{\partial f_1}{\partial x_6}b_2 \\ b_2 \end{bmatrix}$$

$$\Upsilon_1 = c_{11}m_{11}^{-1}f_1 + c_{11}\frac{dm_{11}^{-1}}{dt}x_2 + \frac{\partial f_1}{\partial x_1}m_{11}^{-1}x_2 + \frac{\partial f_1}{\partial x_2}f_1 + \frac{\partial f_1}{\partial x_3}x_4 + \frac{\partial f_1}{\partial x_4}f_2 + \frac{\partial f_1}{\partial x_5}x_6 + \frac{\partial f_1}{\partial x_6}f_3 + \frac{\partial f_1}{\partial x_2}\hat{D}_1 + \frac{\partial f_1}{\partial x_4}\hat{D}_2 + \frac{\partial f_1}{\partial x_6}\hat{D}_3 + k_{12}S_{12} - \frac{\alpha_1 - \alpha_{f1}}{T_1} - c_{11}\frac{dm_{11}^{-1}}{dt}x_{2d} - c_{11}m_{11}^{-1}f_{1d} - \dot{f}_{1d}$$

$\Upsilon_2 = f_3 + k_{22}S_{22} + \hat{D}_3 - \dfrac{\alpha_2 - \alpha_{f2}}{T_2} - \dot{x}_{6d}$

Theorem Considering the underactuated system (4), when $\partial f_1/\partial x_4$ and B are invertible, a set of surface gains k_1, k_2 and the filter time constant vector T satisfying (15), the DSCNDO (25) ensures that the states are uniformly ultimately bounded.

Proof. Selecting Lyapunov function candidate (16), and following the lines of the proof of *Theorem*??, the stability of the NDO is proven in (17). Differentiating both sides of V_2 and replacing (22)-(25) into it, we reach $\dot{V}_2 \leq -(\underline{k_1} - \frac{9}{4})S_1^2 - (\underline{k_2} - \frac{5}{4})S_2^2 - (\frac{1}{\overline{T}} - 2)e^T e + \Delta$, where $\Delta = \varrho^T\varrho/4 + \bar{\kappa}^T\bar{\kappa}/4$, $\varrho, \bar{\kappa}$ are the upper bounds of $|k_1\dot{S}_1|$ and $[(c_1 m_{11}^{-1} + \frac{\partial f_1}{\partial x_2})\tilde{D}_1 + \frac{\partial f_1}{\partial x_4}\tilde{D}_2 + \frac{\partial f_1}{\partial x_6}\tilde{D}_3 + \dot{\tilde{D}}_1, \tilde{D}_3]^T$, respectively. According to the Young's inequality, choosing appropriate parameters k_1, k_2, T to satisfy (15), we have $\dot{V}_2 \leq -2\gamma V_2 + \Delta$. If $V_2(0) \leq p$, $V_2(t) \leq p$. Accordingly, S_1, S_2, e are bounded. So are e_{11}, e_{12}, e_{13}, $e_{21}, e_{22}, \tilde{D}$.

According to the above analysis, the whole system is uniformly ultimately bounded.

Case 3: $\partial f_1/\partial x_3$ and $\partial f_1/\partial x_4$ are present but irreversible at the equilibrium.

Satisfying $\partial f_1/\partial x_3 = 0, \partial f_1/\partial x_4 = 0$ at the equilibrium, the DSCNDOs ((14) and (25)) are invalid. The underactuated system (4) is rewritten as:

$$\dot{X} = F_1(X) + G_1(X)u + G_2(X)d \tag{26}$$

where $F_1 = [m_{11}^{-1}x_2, f_{11}, x_4, f_2, x_6, f_3]^T$, $d = [f_{12} + D_1, D_2, D_3]^T$, G_1 and G_2 are defined in (4). f_{11} includes dissipative and gravity terms. f_{12} includes the cross items vanishing when states converge to the equilibrium. f_{12} is regarded as the uncertainty of the system that can be estimated by the NDO. As $\partial f_{11}/\partial x_4$ or $\partial f_{11}/\partial x_3$ is invertible satisfying *Case* 1 or *Case* 2, *Theorem*?? or *Theorem*3.2 can be applied to this case.

4 Examples

In this section, three examples of underactuated mechanical systems are provided that are attracted a great deal of interest in literature, one each for $C1$, $C2$ and a multi-DOF system that the number of actuated DOFs is higher than that of the underactuated ones. To illustrate the effectiveness of the proposed method, the simulation results controlled by DSCNDO is presented in comparison with those controlled by LQR and DSC.

Example 1: Two-Translational Oscillator with Rotational Actuator The mechanics and symbols of the two-TORA are shown in figure 1. m_i,M_i are the mass of i-th ball and cart respectively; θ_i, τ_i are the swing angle of i-th ball and the torque acting on the i-th ball respectively, where $i = 1, 2$. k_j is the spring coefficient, where $j = 1, 2, 3$.

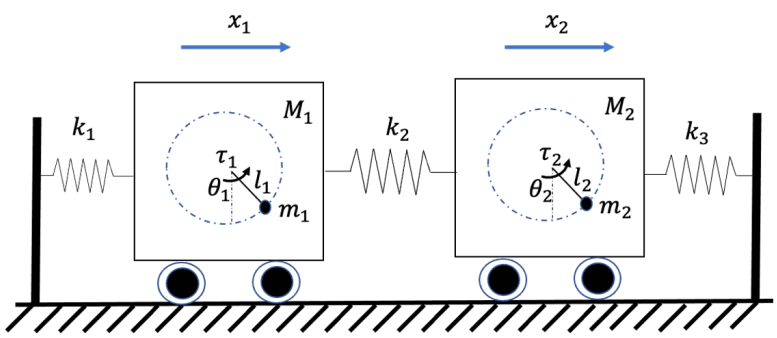

Figure 1: The mechanics of the two-TORA

The dynamics of two-TORA system is modeled as a four-DOF system with two actuators[6].

$$M\ddot{q} + h + \phi = [0, 0, \tau_1, \tau_2]^T + d \tag{27}$$

where

$$M = \begin{bmatrix} M_{11} & 0 & M_{13} & 0 \\ 0 & M_{22} & 0 & M_{24} \\ M_{31} & 0 & M_{33} & 0 \\ 0 & M_{42} & 0 & M_{44} \end{bmatrix}, h = \begin{bmatrix} -m_1 l_1 \sin(\theta_1)\dot{\theta}_1^2 \\ -m_2 l_2 \sin(\theta_2)\dot{\theta}_2^2 \\ m_1 g l_1 \sin(\theta_1) \\ m_2 g l_2 \sin(\theta_2) \end{bmatrix}, \phi = \begin{bmatrix} k_1 x_1 + k_2(x_1 - x_2) \\ k_2(x_2 - x_1) + k_3 x_2 \\ 0 \\ 0 \end{bmatrix}$$

$q = [x_1, x_2, \theta_1, \theta_2]^T$, $M_{11} = M_1 + m_1, M_{13} = m_1 l_1 \cos(\theta_1)$,$M_{22} = M_2 + m_2$, $M_{24} = m_2 l_2 \cos(\theta_2)$, $M_{33} = J_1 + m_1 l_1^2, M_{44} = J_2 + m_2 l_2^2, M_{31} = M_{13}, M_{42} = M_{24}$. $d = [d_1, d_2, d_3, d_4]^T$ is the external disturbance. τ_1, τ_2 are the torques exerting on the system.

Following the lines of coordinate transformation, choose a new coordinate:

$$\begin{aligned} X_1 &= X + \beta(\theta) \\ X_2 &= M_m\dot{X} + M_m\dot{\beta}(\theta) \\ X_3 &= \theta \\ X_4 &= \dot{\theta} \end{aligned} \tag{28}$$

where $X = \begin{bmatrix} x_1 \\ x_2 \end{bmatrix}$, $\theta = \begin{bmatrix} \theta_1 \\ \theta_2 \end{bmatrix}$, $M_m = \begin{bmatrix} M_{11} & 0 \\ 0 & M_{22} \end{bmatrix}$, $\beta(\theta) = M_m^{-1} \begin{bmatrix} m_1 l_1 \sin(\theta_1) \\ m_2 l_2 \sin(\theta_2) \end{bmatrix}$

The dynamics of the two-TORA is converted into a cascade form.

$$\begin{aligned} \dot{X}_1 &= M_m^{-1} X_2 \\ \dot{X}_2 &= f_1 + D_1 \\ \dot{X}_3 &= X_4 \\ \dot{X}_4 &= f_2 + b\tau + D_2 \end{aligned} \tag{29}$$

where $D_1 = [d_1, d_2]^T$, $\tau = [\tau_1, \tau_2]^T$,$f_2$, b ,D_2 are the last two items of $-M^{-1}(h+\phi)$, $M^{-1}b_1$ and $M^{-1}d$, respectively.

$$b_1 = \begin{bmatrix} 0 & 0 \\ 0 & 0 \\ 1 & 0 \\ 0 & 1 \end{bmatrix}, f_1 = K(X_1 - \beta), K = \begin{bmatrix} -(k_1+k_2) & k_2 \\ k_2 & -(k_2+k_3) \end{bmatrix}$$

Clearly, $\partial f_1/\partial X_2 = \partial f_1/\partial X_4 = 0$, $\partial f_1/\partial X_3$ is invertible except at $\theta_1 = \pm\pi/2$ or $\theta_2 = \pm\pi/2$. Actually, the swing angles always satisfy $|\theta_i| < \pi/2$ in practical application.

Based on *Theorem* 1 , we apply the control law (30) to the two-TORA system.

$$\begin{aligned} \tau = -(\frac{\partial f_1}{\partial X_3} b)^{-1}(c_1 M_m^{-1} f_1 + c_2(\frac{\partial f_1}{\partial X_1} M_m^{-1} X_2 + \frac{\partial f_1}{\partial X_3} X_4) + \frac{\partial f_1}{\partial X_1} M_m^{-1} f_1 + \frac{d}{dt}\frac{\partial f_1}{\partial X_3} X_4 + \frac{\partial f_1}{\partial X_3} f_2 \\ +\delta_1 \hat{D}_1 + \delta_2 \hat{D}_2 + K_2 S_2 - T^{-1}(\alpha_1 - \alpha_{f1})) \end{aligned} \tag{30}$$

where

$$\frac{\partial f_1}{\partial X_1} = K, \frac{\partial f_1}{\partial X_3} = -KM_m^{-1} \begin{bmatrix} m_1 l_1 \cos(\theta_1) & 0 \\ 0 & m_2 l_2 \cos(\theta_2) \end{bmatrix}, \frac{d}{dt}\frac{\partial f_1}{\partial X_3} = KM_m^{-1} \begin{bmatrix} m_1 l_1 \sin(\theta_1)\dot{\theta}_1 & 0 \\ 0 & m_2 l_2 \sin(\theta_2)\dot{\theta}_2 \end{bmatrix}$$

Parameters of the two-TORA are set as:

$M_1 = 5.4Kg, m_1 = 0.96Kg, l_1 = 0.6m, J_1 = 0.0022Kg \cdot m^2, M_2 = 6.4Kg, m_2 = 1.26Kg, l_2 = 0.8m, J_2 = 0.0025Kg \cdot m^2, g = 9.8m/s^2, k_1 = 190N/m, k_2 = 100N/m, k_3 = 146N/m.$

and the nonzero initial cart position and rotational angles are : $x_1(0) = 0.2m, x_2(0) = 0.2m, \theta_1(0) = 0.5rad, \theta_2(0) = 0.5rad$. For the position control, the desired value is $x_{1d} = x_{2d} = 0$m, $\theta_{1d} = \theta_{2d} = 0$rad. Moreover, the time-varying disturbance is:

$$d_1(t) = \begin{cases} 0.5\sin(0.5t + \pi/2) & t \in [5\pi, 7\pi]s \\ 0 & others \end{cases}$$
$$d_3(t) = \begin{cases} \sin(0.5t + \pi/2) & t \in [7\pi, 9\pi]s \\ 0 & others \end{cases}$$

In the simulation, $d_1 = d_2, d_3 = d_4$. Considering that $\dot{d} \neq 0$ and $d^{(2)}$ is bounded, $r = 2$ in (5) is used in the NDO design.

The control parameters in (30) are selected as:

$$K_1 = \begin{bmatrix} 14 & 0 \\ 0 & 14 \end{bmatrix}, K_2 = \begin{bmatrix} 10 & 0 \\ 0 & 10 \end{bmatrix}, T = \begin{bmatrix} 0.3 & 0 \\ 0 & 0.1 \end{bmatrix}, c_1 = \begin{bmatrix} 150 & 0 \\ 0 & 150 \end{bmatrix}, c_2 = \begin{bmatrix} 1.5 & 0 \\ 0 & 1.5 \end{bmatrix}$$

and the nonlinear disturbance observer parameter $L_2 = 2L_1$, and L_1 is taken as:

$$L_1 = \begin{bmatrix} l_{11} & l_{12} & 0_{2\times2} & 0_{2\times2} \\ 0_{2\times2} & 0_{2\times2} & l_{21} & l_{22} \end{bmatrix}$$

where $l_{11} = l_{21} = diag([0.2; 0.2]), l_{12} = l_{22} = diag([3; 3])$, $0_{2\times2}$ is a zero matrix with two rows and two columns.

The simulation results are given in Figure 2-4 , one each for the estimation of disturbance, the cart position and the rotation angles of two-TORA system. Simulation results controlled by LQR and DSC are presented as comparison. The quantified results of two-TORA system controlled by three methods are presented in Table 1. It can be observed that all the methods can achieve the desired value with similar performance. The cart can be stabilized efficiently at the equilibrium while the rotational angles converge to zero quickly. Compared to

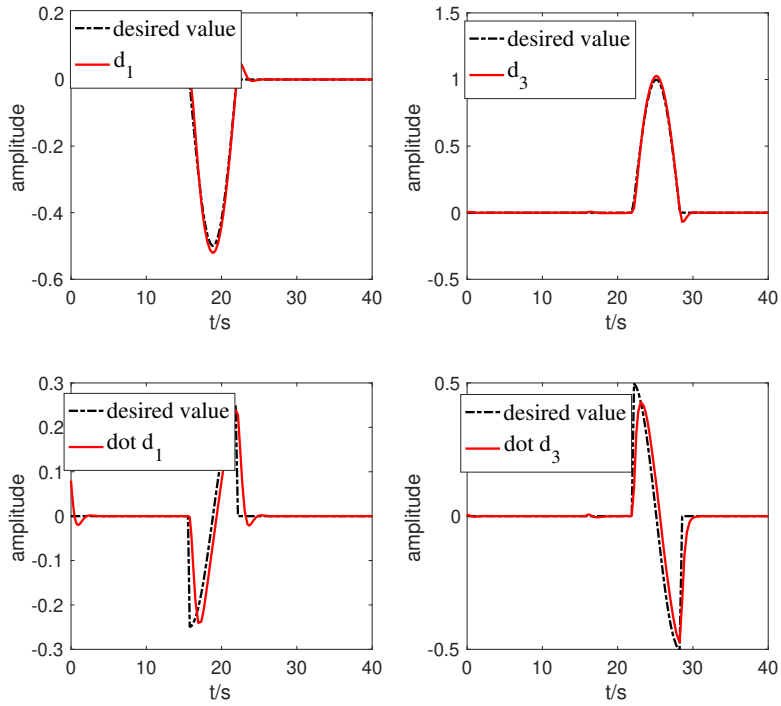

Figure 2: The estimation of disturbance

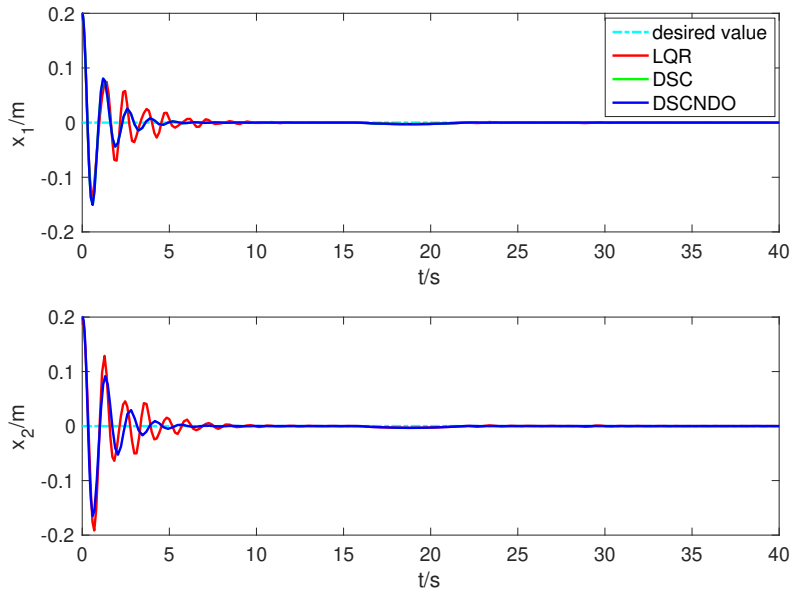

Figure 3: The comparison of the position of carts controlled by DSCNDO with those controlled by DSC and LQR

LQR, the proposed method reaches better transient performance bringing smaller overshoot and settling time. Acting the disturbance from 5πs to 9πs, the disturbance is estimated by the NDO shown in Figure 2. The states controlled by the three controllers can rapidly return to the equilibrium. However, the overshoot controlled by LQR is highest and that controlled by DSCNDO is lowest. It implies that the proposed method has satisfactory robustness.

Remark 3 According to (21), the dynamic surface parameters affect tracking accuracy directly. c_{11}, c_{12} should be chosen appropriately to satisfy the eigenvalues of M negative. Then, adjust the parameters to make the minimum eigenvalue of M as big as possible to ensure the state error small. On the other hand, choose proper K_1, K_2, T to ensure (15) satisfied. In addition, the filtering error is liable to cause system instability. Therefore, the time constant should be chosen carefully.

Example 2: Crane The mechanics of crane is shown in Figure 5 and the dynamics is given by:

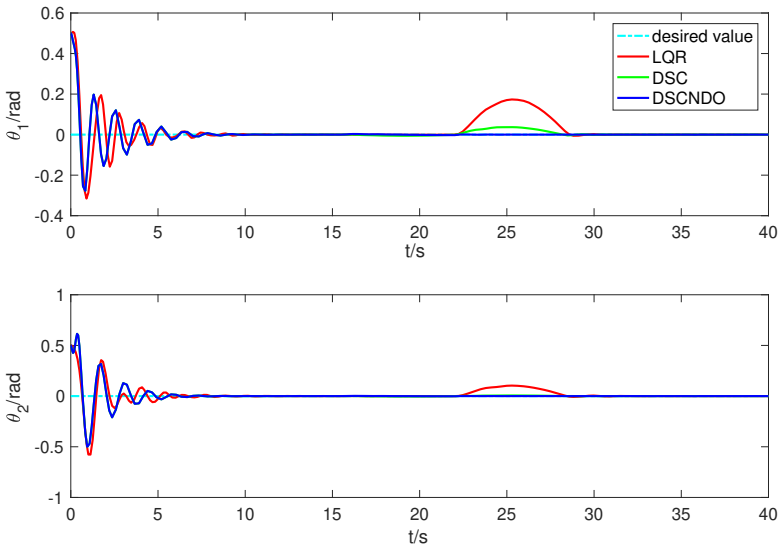

Figure 4: The comparison of the angles of balls controlled by DSCNDO with those controlled by DSC and LQR

Table 1: The quantified results of two-TORA controlled by three methods

Methods	$t_{sx1}(s)$	$t_{sx2}(s)$	$t_{s\theta_1}(s)$	$t_{s\theta_2}(s)$	$\lvert x_{1max}\rvert(m)$	$\lvert x_{2max}\rvert(m)$	$\lvert\theta_{1max}\rvert(rad)$	$\lvert\theta_{2max}\rvert(rad)$
	$\Delta \leq 1cm$		$\Delta \leq 0.01rad$		with disturbance			
LQR	4.85	6.02	7.44	9.89	0	0	0.17	0.10
DSC	**3.26**	**3.50**	**7.07**	**9.44**	0	0	0.04	**0**
DSCNDO	**3.26**	**3.50**	**7.07**	**9.44**	0	0	**0**	**0**

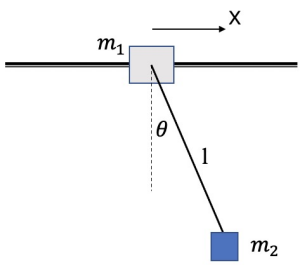

Figure 5: The mechanics of the crane system

$$\begin{aligned}&(m_1+m_2)\ddot{x}+m_2l\cos(\theta)\ddot{\theta}+m_2l\sin(\theta)\dot{\theta}^2=\tau+d_3\\&\cos(\theta)\ddot{x}+l\ddot{\theta}+g\sin(\theta)=d_1\end{aligned}\tag{31}$$

Choose a new coordinate: $x_1 = x+\beta$, $x_2 = \dot{x}+l\dot{\theta}/\cos(\theta)$,$x_3=\theta$,$x_4=\dot{\theta}$, where $\beta = l\cdot\ln|\sec(\theta)+\tan(\theta)|$. Utilizing the global change of the coordinates (2), the dynamics of the crane can be written as:

$$\begin{aligned}\dot{x}_1&=x_2\\\dot{x}_2&=f_1+d_1\\\dot{x}_3&=x_4\\\dot{x}_4&=f_2+b_1\tau+D_2\end{aligned}\tag{32}$$

where $f_1=-g\tan(x_3)+\tan(x_3)/\cos(x_3)x_4^2$, b_1, f_2, D_2 are given in (3) for $C2$.

Obviously, $\partial f_1/\partial x_4$ is irreversible at the original point satisfying $Case$ 3. We divide f_1 into two parts.

$$f_1=\underbrace{-g\tan(x_3)}_{f_{11}}+\underbrace{\tan(x_3)/\cos(x_3)\dot{x}_3^2}_{f_{12}}$$

Based on (26), $D_1=f_{12}+d_1$. $\partial f_{11}/\partial x_3$ is invertible and $\partial f_{11}/\partial x_4=0$. Apply $Theorem$**??** to the crane system. Parameters are selected as: $m_1=1Kg$, $m_2=0.1Kg$, $l=1m$, $g=9.8N/Kg$. d_1 and d_3 are defined in $example1$.

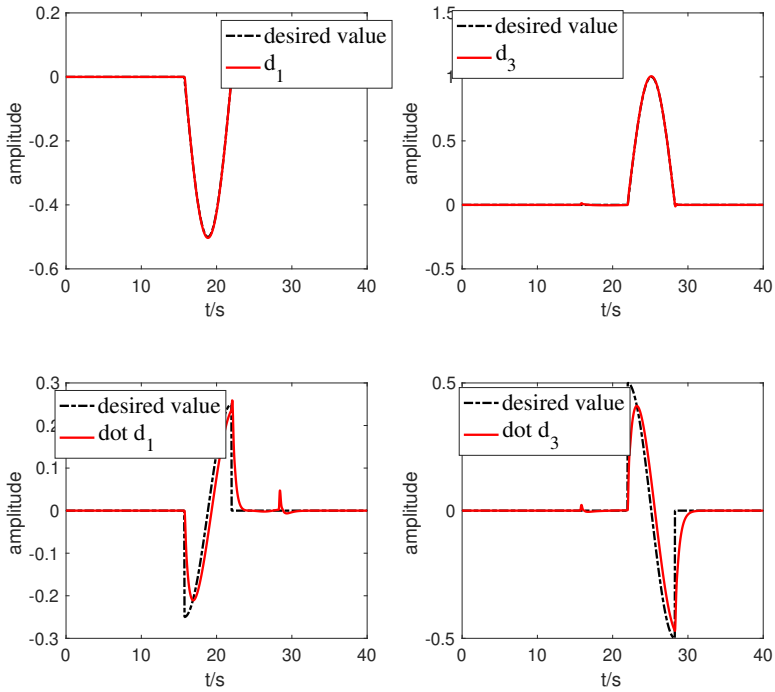

Figure 6: The estimation of disturbance

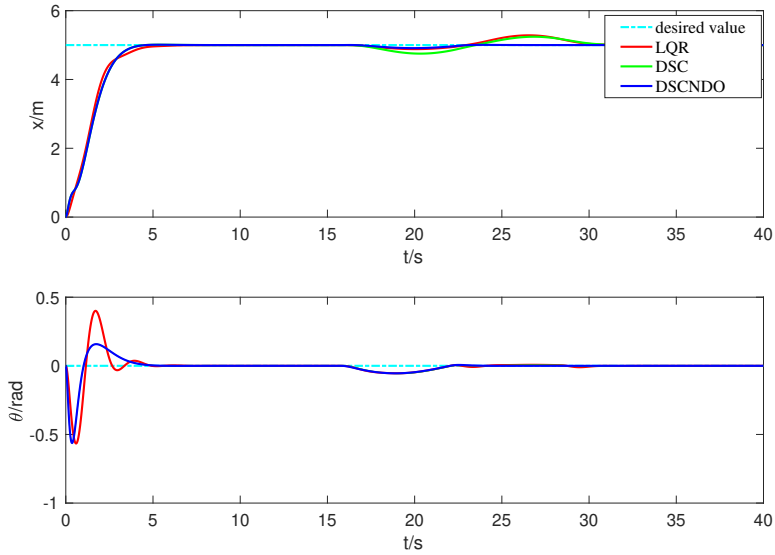

Figure 7: The comparison of three methods on the crane system with disturbance

Table 2: The quantified results of Crane controlled by three methods

Methods	$t_{sx}(s)$	$t_{s\theta}(s)$	$\lvert x_{max}\rvert(m)$	$\lvert\theta_{max}\rvert(rad)$
	$\Delta \leq 1cm$	$\Delta \leq 0.01rad$	with disturbance	
LQR	6.45	4.63	0.28	**0.05**
DSC	**5.97**	**4.31**	0.22	**0.05**
DSCNDO	**5.97**	**4.31**	**0.04**	**0.05**

The estimation of disturbance and performance is presented in Figure6 -7 and Table 2. It is shown that all the methods can drive the underactuated crane system to the desired value. However, better performance is obtained by the proposed method. The load's swing decreases with smaller residual angle. Furthermore,

the settling time of the proposed method is less than that of LQR. The system controlled by DSCNDO also possesses satisfactory stability when acting disturbance.

Remark 4 In crane control, the swing angle always satisfies $-\pi/2 < \theta < \pi/2$. The trolley is expected to gradually reach the desired position without overshoot while the load oscillates as small as possible.

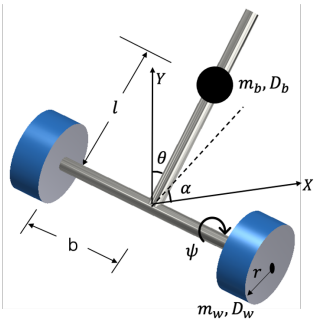

Figure 8: The mechanics of the wheeled inverted pendulum

Example 3: Wheeled Inverted Pendulum The mechanics of the WIP is presented in Figure 8. It is noticed that the WIP is a three-DOF mechanics with an underactuated inclination angle. The dynamics is given [10]:

$$m(q)\ddot{q} + h(q,\dot{q}) + \phi(\dot{q}) = \tau + d \tag{33}$$

where $q = [q_1, q_2, q_3]^T = [\psi, \theta, \alpha]^T$ denotes the rotation angle of the wheels, inclination angle of the body and yaw angle of the WIP, respectively.

$$m(q) = \begin{bmatrix} m_{11} & m_{12} & m_{13} \\ m_{21} & m_{22} & m_{23} \\ m_{31} & m_{32} & m_{33} \end{bmatrix}, h(q,\dot{q}) = \begin{bmatrix} h_1 \\ h_2 \\ h_3 \end{bmatrix}, \phi(\dot{q}) = \begin{bmatrix} 2D_w\dot{q}_1 \\ 2D_b(\dot{q}_2 - \dot{q}_1) \\ \frac{2b^2}{r^2}(D_b + D_w)\dot{q}_3 \end{bmatrix}, \tau = \begin{bmatrix} 0 \\ \tau_1 \\ \tau_2 \end{bmatrix}$$

where $m_{11} = a + b\cos(q_2), m_{12} = b\cos(q_2) + c$, $m_{21} = b\cos(q_2), m_{22} = c, m_{33} = I_{bl}\sin^2(q_2) + \frac{2b^2}{r^2}(I_{wa} + m_w r^2)$, $m_{13} = m_{23} = m_{31} = m_{32} = 0$,$a = (m_b + 2m_w)r^2 + 2I_{wa}, b = m_b l r$, $c = m_b l^2 + I_{by}, I_{bl} = I_{bz} + m_b l^2$, $h_1 = -b\sin(q_2)(\dot{q}_2^2 + \dot{q}_3^2) - I_{bl}\sin(q_2)\cos(q_2)\dot{q}_3^2 - G\sin(q_2)$, $h_2 = -I_{bl}\sin(q_2)\cos(q_2)\dot{q}_3^2 - G\sin(q_2)$, $h_3 = 2I_{bl}\sin(q_2)\cos(q_2)\dot{q}_2\dot{q}_3 + b\sin(q_2)\dot{q}_1\dot{q}_3$, $G = m_b g l$

Choose a new coordinate: $x_1 = x + \beta$, $x_2 = m_{11}\dot{q}_1 + m_{12}\dot{q}_2$, $x_3 = q_2$, $x_4 = \dot{q}_2$, $x_5 = q_3$, $x_6 = \dot{q}_3$, where $\beta = q_2 + \frac{c-a}{\sqrt{a^2-b^2}}\arctan(\sqrt{\frac{a-b}{a+b}}\tan(\frac{q_2}{2})$. Based on (3), the dynamic model (33) can be rewritten as

$$\begin{aligned} \dot{x}_1 &= m_{11}^{-1}x_2 \\ \dot{x}_2 &= f_{11} + f_{12} + D_1 \\ \dot{x}_3 &= x_4 \\ \dot{x}_4 &= f_2 + b_1 u + D_2 \\ \dot{x}_5 &= x_6 \\ \dot{x}_6 &= f_3 + b_2 u + D_3 \end{aligned}$$

where $f_{11} = G_b\sin(x_3) - 2D_w m_{11}^{-1}(x_2 - m_{12}x_4)$, $f_{12} = b\sin(x_3)(x_4^2 + x_6^2) + I_{bl}\sin(x_3)\cos(x_3)x_6^2$

Obviously, $\partial f_{11}/\partial x_4$ is existed and invertible. Based on $Theorem 3.2$, the control law (25) is applied to the WIP.

Table 3: The quantified results of MIP controlled by three methods

Methods	$t_{s\phi}(s)$	$t_{s\theta}(s)$	$t_{s\alpha}(s)$	$\lvert\phi_{max}\rvert(rad)$	$\lvert\theta_{max}\rvert(rad)$	$\lvert\alpha_{max}\rvert(rad)$
	$\Delta \leq 0.01rad$			with disturbance		
LQR	**4.45**	4.45	14.05	0.77	**0.22**	0.06
DSC	**4.45**	**4.29**	**0.43**	0.67	0.32	0.20
DSCNDO	**4.45**	**4.29**	**0.43**	**0.36**	0.27	**0**

The physical parameters are presented as: $m_b = 2.58Kg, I_{by} = 0.00177Kg \cdot m^2, I_{bz} = I_{by}, I_{wa} = 0.00014Kg \cdot m^2, I_{wd} = 0.00084Kg \cdot m^2, D_w = 0.8N \cdot s/m, m_w = 0.14Kg, l = 0.0622m, b = 0.15m, r = 0.04m, D_b = 0.5m, g = 9.8N/Kg$. The control parameters are selected as: $k_{11} = k_{21} = 20, k_{12} = k_{22} = 20, T_1 = T_2 = 0.01, c_{11} = 3$. The initial states are chosen as: $q_1(0) = 0.3, q_2(0) = -0.5, q_3(0) = 0.3, \dot{q}_1(0) = 2, \dot{q}_2(0) = \dot{q}_3(0) = 0$. The disturbance is selected as $d = [d_1, d_1, d_3]^T$, where d_1, d_3 are defined in *example 1* .The estimation of disturbance and performance are presented in Figure 9-10 blue and Table 3. It is observed the proposed method can stabilize the

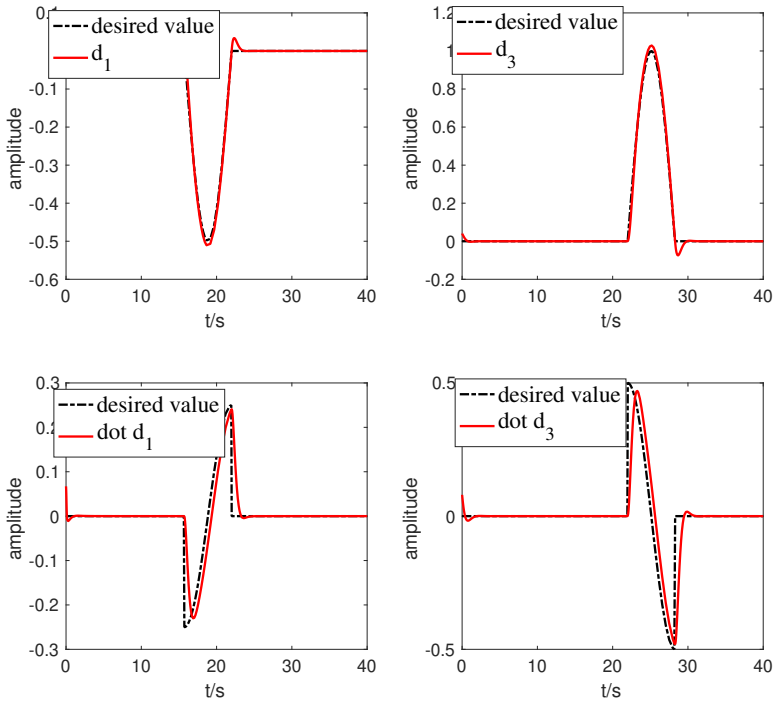

Figure 9: The estimation of disturbance

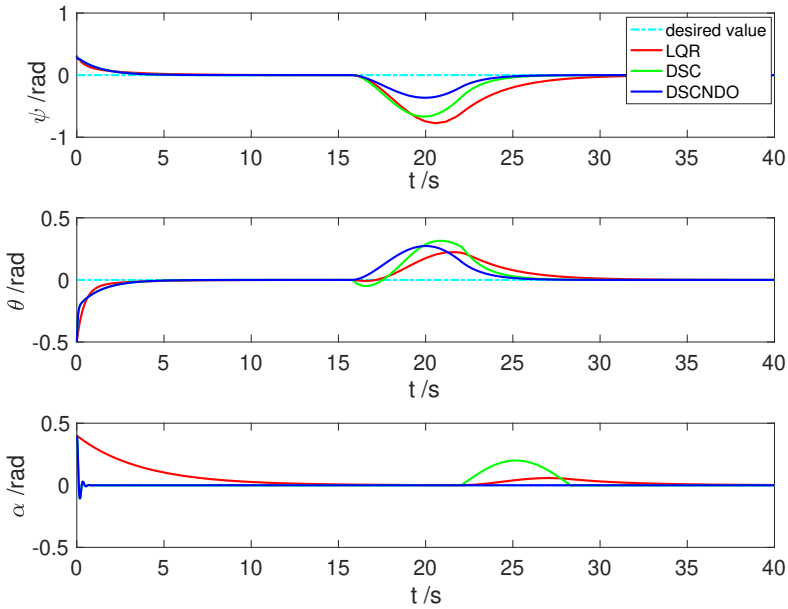

Figure 10: The comparison of three methods on the MWIP system with disturbance

WIP with better performance than those controlled by DSC and LQR.

5 Conclusion

In this paper, we propose an NDO-based DSC strategy overcoming chattering problem of SMC and the phenomenon of "explosion" in a highly complicated control law while using backstepping. It also solves the computation feasibility problem when a dynamic model includes cross terms. The novel DSCNDO strategy is generalized to underactuated systems derived by Lagrangian method. Lyapunov-based analysis is used to analyze the stability of system and it is proven that the states are uniformly ultimately bounded. The control

strategy is applied to underactuated systems such as two-TORA, Crane and WIP. Several examples and comparisons are proposed to demonstrate the effectiveness of the proposed method. It is implied that the proposed DSCNDO yields satisfactory performance.

Data Availability Statement

The data that support the findings of this study are available from the corresponding author upon reasonable request.

References

[1] Spong MW. The swing up control problem for the Acrobot. *IEEE Control Systems Magazine* 1995; 15(1): 49-55.

[2] Ding F, Huang J, Wang Y, Zhang J, He S. Sliding mode control with an extended disturbance observer for a class of underactuated system in cascaded form. *Nonlinear Dynamics* 2017; 90(4): 2571–2582.

[3] Cabecinhas D, Cunha R, Silvestre C. A trajectory tracking control law for a quadrotor with slung load. *Automatica* 2019; 106: 384 - 389.

[4] Vandanipour M, Khodabandeh M. Adaptive fractional order sliding mode control for a quadrotor with a varying load. *Aerospace science and technology* 2019; 86: 737-747.

[5] Ye H. Stabilization of Uncertain Feedforward Nonlinear Systems With Application to Underactuated Systems. *IEEE Transactions on Automatic Control* 2019; 64(8): 3484-3491.

[6] Wu Y, Sun N, Fang Y, Liang D. An Increased Nonlinear Coupling Motion Controller for Underactuated Multi-TORA Systems: Theoretical Design and Hardware Experimentation. *IEEE Transactions on Systems, Man, and Cybernetics: Systems* 2019; 49(6): 1186-1193.

[7] Xu R, Özgüner Ü. Sliding mode control of a class of underactuated systems. *Automatica* 2008; 44(1): 233 - 241.

[8] Ding F, Huang J, Wang Y, Matsuno T, Fukuda T. Vibration damping in manipulation of deformable linear objects using sliding mode control. *Advanced Robotics* 2014; 28(3): 157-172.

[9] Yue M, An C, Li Z. Constrained Adaptive Robust Trajectory Tracking for WIP Vehicles Using Model Predictive Control and Extended State Observer. *IEEE Transactions on Systems, Man, and Cybernetics: Systems* 2018; 48(5): 733-742.

[10] Huang J, Zhang M, Ri S, Xiong C, Li Z, Kang Y. High-Order Disturbance-Observer-Based Sliding Mode Control for Mobile Wheeled Inverted Pendulum Systems. *IEEE Transactions on Industrial Electronics* 2020; 67(3): 2030-2041.

[11] Wang S, Fu M, Wang Y. Robust adaptive steering control for unmanned surface vehicle with unknown control direction and input saturation. *International Journal of Adaptive Control and Signal Processing* 2019; 33(7): 1212-1224.

[12] Park BS, Kwon JW, Kim H. Neural network-based output feedback control for reference tracking of underactuated surface vessels. *Automatica* 2017; 77: 353 - 359.

[13] Han SI, Lee JM. Partial Tracking Error Constrained Fuzzy Dynamic Surface Control for a Strict Feedback Nonlinear Dynamic System. *IEEE Transactions on Fuzzy Systems* 2014; 22(5): 1049-1061.

[14] Wang H, Li Y, Liu K. Globally Stable Adaptive Dynamic Surface Control for Cooperative Path Following of Multiple Underactuated Autonomous Underwater Vehicles. *Asian Journal of Control* 2018; 20(3): 1204-1220.

[15] Chang Y, Chan W, Chang C. T-S Fuzzy Model-Based Adaptive Dynamic Surface Control for Ball and Beam System. *IEEE Transactions on Industrial Electronics* 2013; 60(6): 2251-2263.

[16] Dian S, Chen L, Hoang S, Zhao T, Tan J. Gain scheduled dynamic surface control for a class of underactuated mechanical systems using neural network disturbance observer. *Neurocomputing* 2018; 275: 1998 - 2008.

[17] Mobayen S. Design of LMI-based sliding mode controller with an exponential policy for a class of underactuated systems. *Complexity* 2016; 21(5): 117-124.

[18] Du C, Yang C, Li F, Gui W, Li W. Design and Implementation of Observer-Based Sliding Mode for Underactuated Rendezvous System. *IEEE Transactions on Systems, Man, and Cybernetics: Systems* 2019; 51(10): 6003 - 6014.

[19] Rsetam K, Cao Z, Man Z. Cascaded-Extended-State-Observer-Based Sliding-Mode Control for Underactuated Flexible Joint Robot. *IEEE Transactions on Industrial Electronics* 2020; 67(12): 10822-10832.

[20] Huang J, Ri S, Fukuda T, Wang Y. A Disturbance Observer Based Sliding Mode Control for a Class of Underactuated Robotic System With Mismatched Uncertainties. *IEEE Transactions on Automatic Control* 2019; 64(6): 2480-2487.

[21] Wang N, Er MJ. Direct Adaptive Fuzzy Tracking Control of Marine Vehicles With Fully Unknown Parametric Dynamics and Uncertainties. *IEEE Transactions on Control Systems Technology* 2016; 24(5): 1845-1852.

[22] Bessa WM, Otto S, Kreuzer E, Seifried R. An adaptive fuzzy sliding mode controller for uncertain underactuated mechanical systems. *Journal of Vibration and Control* 2019; 25(9): 1521-1535.

[23] Weng Y, Wang N. Data-driven robust backstepping control of unmanned surface vehicles. *International Journal of Robust and Nonlinear Control* 2020; 30(9): 3624-3638.

[24] Azimi MM, Koofigar HR. Adaptive fuzzy backstepping controller design for uncertain underactuated robotic systems. *Nonlinear Dynamics* 2015; 79(2): 1457–1468.

[25] Pucci D, Romano F, Nori F. Collocated Adaptive Control of Underactuated Mechanical Systems. *IEEE Transactions on Robotics* 2015; 31(6): 1527-1536.

[26] Ouyang H, Xu X, Zhang G. Tracking and load sway reduction for double-pendulum rotary cranes using adaptive nonlinear control approach. *International Journal of Robust and Nonlinear Control* 2020; 30(5): 1872-1885.

[27] Chen X, Zhao H, Sun H, Zhen S, Mamun AA. Optimal Adaptive Robust Control Based on Cooperative Game Theory for a Class of Fuzzy Underactuated Mechanical Systems. *IEEE Transactions on Cybernetics* 2020; 52(5): 3632-3644.

[28] Swaroop D, Hedrick JK, Yip PP, Gerdes JC. Dynamic surface control for a class of nonlinear systems. *IEEE Transactions on Automatic Control* 2000; 45(10): 1893-1899.

[29] Zhang T, Xia M, Yi Y, Shen Q. Adaptive Neural Dynamic Surface Control of Pure-Feedback Nonlinear Systems With Full State Constraints and Dynamic Uncertainties. *IEEE Transactions on Systems, Man, and Cybernetics: Systems* 2017; 47(8): 2378-2387.

[30] Zhang T, Xu H. Adaptive optimal dynamic surface control of strict-feedback nonlinear systems with output constraints. *International Journal of Robust and Nonlinear Control* 2020; 30(5): 2059-2078.

[31] Wu J, Huang J, Wang Y, Xing K. Nonlinear Disturbance Observer-Based Dynamic Surface Control for Trajectory Tracking of Pneumatic Muscle System. *IEEE Transactions on Control Systems Technology* 2014; 22(2): 440-455.

[32] Liu H, Pan Y, Cao J. Composite Learning Adaptive Dynamic Surface Control of Fractional-Order Nonlinear Systems. *IEEE Transactions on Cybernetics* 2020; 50(6): 2557-2567.

[33] Huang J, Ri S, Liu L, Wang Y, Kim J, Pak G. Nonlinear Disturbance Observer-Based Dynamic Surface Control of Mobile Wheeled Inverted Pendulum. *IEEE Transactions on Control Systems Technology* 2015; 23(6): 2400-2407.

[34] Chen T, Shan J. Distributed Tracking of a Class of Underactuated Lagrangian Systems With Uncertain Parameters and Actuator Faults. *IEEE Transactions on Industrial Electronics* 2020; 67(5): 4244-4253.

[35] Gutiérrez-Oribio D, Mercado-Uribe JA, Moreno JA, Fridman L. Robust global stabilization of a class of underactuated mechanical systems of two degrees of freedom. *International Journal of Robust and Nonlinear Control* 2021; 31(9): 3908-3928.

[36] Wen-Hua Chen . Disturbance observer based control for nonlinear systems. *IEEE/ASME Transactions on Mechatronics* 2004; 9(4): 706-710.

[37] Zou Y, Cheng KWE, Cheung NC, Pan JF. A Polymer-Based Air Gap Length Prediction Method With Current Injection and Fuzzy Logic Observer. *IEEE Transactions on Magnetics* 2017; 53(11): 1-4.

[38] Jeong S, Ji D, Park JH, Won S. Adaptive synchronization for uncertain chaotic neural networks with mixed time delays using fuzzy disturbance observer. *Applied Mathematics and Computation* 2013; 219(11): 5984 - 5995.

[39] Rabiee H, Ataei M, Ekramian M. Continuous nonsingular terminal sliding mode control based on adaptive sliding mode disturbance observer for uncertain nonlinear systems. *Automatica* 2019; 109: 108515.

[40] Olfati-Saber R. Normal forms for underactuated mechanical systems with symmetry. *IEEE Transactions on Automatic Control* 2002; 47(2): 305-308.